



HAL
open science

Low-Temperature Rate Constants and Product-Branching Ratios for the C(1 D) + H 2 O Reaction

Kevin Hickson

► **To cite this version:**

Kevin Hickson. Low-Temperature Rate Constants and Product-Branching Ratios for the C(1 D) + H 2 O Reaction. Journal of Physical Chemistry A, 2019, 123 (25), pp.5206-5213. 10.1021/acs.jpca.9b03037 . hal-02322215

HAL Id: hal-02322215

<https://hal.science/hal-02322215>

Submitted on 11 Jan 2021

HAL is a multi-disciplinary open access archive for the deposit and dissemination of scientific research documents, whether they are published or not. The documents may come from teaching and research institutions in France or abroad, or from public or private research centers.

L'archive ouverte pluridisciplinaire **HAL**, est destinée au dépôt et à la diffusion de documents scientifiques de niveau recherche, publiés ou non, émanant des établissements d'enseignement et de recherche français ou étrangers, des laboratoires publics ou privés.

Low Temperature Rate Constants and Product Branching Ratios for the $C(^1D) + H_2O$ Reaction

Kevin M. Hickson^{*,a,b}

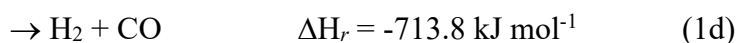
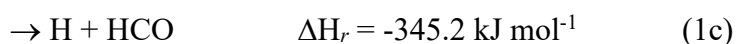
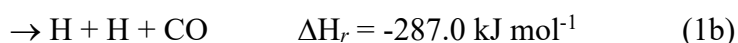
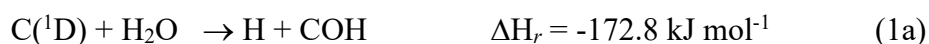
^a*Université de Bordeaux, Institut des Sciences Moléculaires, F-33400 Talence, France*

^b*CNRS, Institut des Sciences Moléculaires, F-33400 Talence, France*

Abstract: The gas-phase reaction between atomic carbon in its first electronically excited 1D state and water has been studied over the 50-296 K temperature range using a supersonic flow apparatus. $C(^1D)$ atoms were produced by pulsed ultraviolet multiphoton dissociation of carbon tetrabromide; a process which also generates ground state atomic carbon $C(^3P)$. The reaction was followed by detecting product H-atoms by pulsed vacuum ultraviolet laser induced fluorescence. Two types of experiment were performed. Firstly, temperature dependent rate constants were derived by recording H-atom formation curves at various gas-phase water concentrations at each temperature. Secondly, temperature dependent H-atom yields were extracted by comparing the H-atom fluorescence intensities generated by the target $C(^1D) + H_2O$ reaction with those of a reference reaction. The second-order rate constants are large and increase to low temperature, while the measured H-atom yields are close to the theoretical maximum value of 2 above 100 K. At 50 K, neither rate constants nor H-atom yields could be derived due to H-atom formation by quantum tunneling in the activated $C(^3P) + H_2O$ reaction. The present results are discussed in the context of earlier work on the $C(^1D)/C(^3P) + H_2O$ reactions.

1 Introduction

The gas-phase reactions of neutral atomic carbon are important in many different environments ranging from those at high temperature, such as combustion systems to those at lower temperature, such as planetary atmospheres and in the interstellar medium. Given the wide application of these processes, numerous studies¹⁻¹³ examining the chemistry of ground state atomic carbon in its ground electronic state, C(³P), are available, providing both kinetic and dynamic information regarding their reactivity towards a wide variety of molecular coreagents. In contrast, studies of the gas-phase chemistry of excited state C(¹D) atoms are much less common, with one notable exception being the C(¹D) + H₂ reaction, a prototypical insertion type reaction allowing comparison between the results of state-selected dynamics experiments¹⁴⁻¹⁶, and detailed quantum mechanical calculations¹⁷⁻²⁶. While several dynamics studies have been reported for other C(¹D) atom reactions over a range of conditions,^{13, 27-30} until recently most of the kinetic investigations of C(¹D) reactivity had only been performed at room temperature.³¹⁻³⁶ Over the past few years, this issue has been addressed through a series of kinetic investigations of the low temperature reactions of excited state atomic carbon with stable molecules (CH₃OH,⁷ H₂,³⁷ D₂,³⁸ HD,³⁹ CH₄,⁴⁰ C₂H₆,⁴⁰ NO,⁴¹ O₂,⁴¹ CO₂⁴²) as well as non-reactive processes such as the quenching of C(¹D) atoms by N₂.⁴³ The present study builds on this earlier work by tackling the reactivity of C(¹D) atoms with water, a system which has several possible exothermic exit channels at low temperature in the gas-phase.⁴⁴



Although this reaction is unlikely to play an important role in the gas phase interstellar medium given its short radiative lifetime (compared to the time between collisions), it might contribute to the chemistry of planetary atmospheres containing water vapour. Water is thought to be deposited in the atmosphere of Titan through the ablation of micrometeorites in the upper atmosphere.⁴⁵ Photochemical models of Titan's atmosphere⁴⁶ predict that C₃ molecules could reach high abundances at these altitudes which are expected to photodissociate to produce atomic carbon in either the ground triplet or excited singlet state.

There have been several previous calculations of the potential energy surfaces (PESs) involved in the reaction of carbon atoms with water^{4, 44, 47-49} beginning with the early work of Ahmed et al.⁴⁹ who concluded that ground triplet state carbon atoms are unreactive towards water. Hwang et al.⁴⁷ performed an ab initio study of the PESs for the reactions of both C(³P) and C(¹D) with H₂O at various levels of theory including CCSD(T)/6-311+G(3df,2p), MP2/6-31G(d,p) and QCISD/6-311G(d,p). They determined that both reactions occurred initially via the formation of prereactive C-OH₂ complexes. In the case of the C(³P) + H₂O reaction, hydrogen atom transfer leading to HCOH formation was predicted to involve a barrier of 46 kJ mol⁻¹. For the C(¹D) + H₂O reaction this barrier was predicted to be below the reagent level with the transition state (TS) located at -25 kJ mol⁻¹ and therefore this process was considered to be potentially fast at low temperatures. Ozkan and Dede⁴⁴ also performed a theoretical investigation of both of these reactions using CASSCF-MCQDPT2, CCSD and DFT methodologies. These authors could not locate the TS for channel (1d) leading to H₂ and CO products, concluding that this pathway was unlikely to exist. They predicted that the major products of both the C(³P)/ C(¹D) + H₂O reactions should mostly be CO + H + H (channel (1b)) given the large exothermicity of the possible product channels (with any HCO or COH formed in channels (1a) and (1c) subsequently dissociating to H + CO). Schreiner and Reisenauer studied the C(³P)/C(¹D) + H₂O reactions both experimentally and theoretically. They performed

a matrix isolation study of these reactions by co-condensing carbon atoms from laser ablated graphite and water vapour diluted in argon at 10 K. They also calculated the relevant PESs for the reaction of atomic carbon at the CCSD(T)/cc-pVTZ+ZPVE level of theory. In line with previous work, they concluded that C(³P) does not react with H₂O and that crossings between the triplet and singlet surfaces were unimportant.

In terms of earlier kinetic studies of the reactions of C(³P)/C(¹D) + H₂O reactions, most previous work has been performed at room temperature. Measurements by Husain and Kirsch⁵⁰ and later, by Husain and Young⁵¹ of the kinetics of the C(³P) + H₂O reaction at room temperature provided only upper limits for the rate constant of $< 10^{-12} \text{ cm}^3 \text{ s}^{-1}$ and $\leq 3.6 \times 10^{-13} \text{ cm}^3 \text{ s}^{-1}$ respectively, in good agreement with the conclusions of ab initio calculations. Nevertheless, an investigation of the kinetics of the C(³P) + H₂O and C(³P) + D₂O reactions to temperatures as low as 50 K by Hickson et al.⁴, has shown that despite the presence of an activation barrier for these process, the rate constants increase dramatically below 100 K as a result of quantum tunneling, reaching values as high as $3.6 \times 10^{-11} \text{ cm}^3 \text{ s}^{-1}$ at 50 K. The role of tunneling in these reactions was clarified through direct measurements of H- and D- atom product formation. By comparing these H-/D-atom yields with those of a reference reaction with a known H-atom yield (the C(³P) + C₂H₄ → C₃H₃ + H reaction), these authors were able to establish quantitative yields for product formation. Interestingly, while the H-atom yield of the C(³P) + H₂O reaction was seen to be less than unity, D-atom yields for the C(³P) + D₂O reaction were a factor of two smaller again, confirming the expected lower tunneling efficiency of deuterium with respect to hydrogen. Husain and Kirsch also studied the kinetics of the C(¹D) + H₂O reaction at room temperature.³³ Despite problems associated with water photolysis in their system leading to only a limited measurement accuracy, they found a significantly larger rate constant of $1.7 \times 10^{-11} \text{ cm}^3 \text{ s}^{-1}$ for this process than the corresponding one for the C(³P) +

H₂O reaction. No other kinetic studies of the C(¹D) + H₂O reaction have been performed at room temperature or otherwise.

To address this issue, kinetic measurements of the C(¹D) + H₂O reaction were performed over the range 50 - 296 K. In this work, rate constants and product yields of the H-atom formation channels of this reaction were measured as a function of temperature. Section 2 outlines the experimental techniques used to perform the experiments, while section 3 presents the results obtained and discusses this work in the context of earlier experimental and theoretical studies. The conclusions are described in section 4.

2 Experimental Methods

A continuous supersonic flow reactor employing axisymmetric Laval nozzles was used to perform the experiments. As this method is explained in earlier papers,^{52, 53} only features specific to this work are described here. Three Laval nozzles were used in the present investigation based on the use of argon as the carrier gas, providing gas flows with characteristic temperatures of 50 K, 75 K and 127 K. Only argon based nozzles could be used in this study due to the efficient quenching of C(¹D) atoms by N₂,⁴³ the carrier gas employed in all other nozzles available. Flow characteristics for the nozzles used here are summarized in Table 1 of Grondin et al.⁵⁴ Room temperature measurements (296 K) were also performed by removing the Laval nozzle, using argon as the carrier gas.

C(¹D) atoms were produced by the 266 nm pulsed multiphoton dissociation of CBr₄ for these experiments. This process is also known to produce C(³P) atoms as the major photolysis product with a C(¹D)/C(³P) ratio of 0.1 - 0.15.⁷ Solid CBr₄ was contained in a flask at room temperature and a known fixed pressure. Its vapour was carried into the reactor itself by a small argon flow diverted through the vessel. The concentration of CBr₄ molecules within the cold supersonic flow was estimated to be less than 2×10^{13} cm⁻³. A controlled evaporation mixing system was used to introduce water in the experiment in an identical manner to the study of Hickson et al.⁴

Briefly, liquid water was flowed from a reservoir through a liquid flow meter (values of 0.1-1.2 g hr⁻¹ were used for the present experiments) into an evaporation device (controlled evaporation mixing system, CEM) maintained at a temperature of 373 K. A small fraction of the total Ar gas flow (~700 sccm) was passed into the CEM to carry the water vapour into the reactor. The output of the CEM was connected to a 10 cm long cell with UV grade quartz windows which was continuously irradiated by the output of a pen-ray mercury lamp. This allowed us to measure gas-phase H₂O quantitatively by absorption by recording the transmission of the 185 nm mercury line in the presence and absence of H₂O (I and I₀ respectively) with a channel photomultiplier (CPM) operating in photon counting mode. The cell pressure was maintained in the range 700-800 Torr, allowing significant absorption for even the smallest [H₂O]. The other intense atomic mercury lines (notably the 254 nm line) were blocked by a narrow-band interference filter centered at 185 nm placed in front of the CPM. A value of 6.78×10^{-20} cm² was used for the H₂O absorption cross-section at this wavelength,⁵⁵ allowing us to calculate the water vapour concentration through the Beer-Lambert law. The cell output was connected to the reservoir via a tube heated to 353 K to prevent condensation losses. No additional upstream losses were considered as the water vapour was diluted fivefold upon entering the Laval nozzle reservoir.

Unfortunately, it was not possible to follow C(¹D) decays directly due to a lack of an appropriately sensitive method to probe these atoms. Instead, product H(²S) atoms were detected through vacuum ultraviolet laser induced fluorescence (VUV LIF) at 121.567 nm. The generation and detection of this tunable radiation has already been described in other recent work.^{4, 5, 7, 8, 37, 39, 40-43, 56} As recent experiments have determined that the C(³P) + H₂O → H + HCO reaction occurs by tunneling at temperatures below 100 K,⁴ it was necessary to establish whether this reaction might affect the investigation of the corresponding C(¹D) reaction. Indeed, as the reaction kinetics are followed through H-atom VUV LIF, it was possible that H-atoms

produced by the ground state atomic carbon reaction could interfere with the kinetics of H-atom formation by the excited state atomic carbon reaction at the lowest temperatures. The various tests that were performed to check this effect are described in section 3.

The gases used in the experiments (Ar 99.999%, Kr 99.99%) were not purified. Ar carrier gas was passed into mass-flow controllers directly from the cylinder, allowing precise control over the water vapor and precursor molecule concentrations in the cold flow upstream of the Laval nozzle. The mass-flow controllers themselves were calibrated prior to use by flowing Ar into a known volume while recording the pressure change as a function of time.

3 Results and Discussion

Temperature dependent rate constants

An excess of H₂O molecules with respect to C(¹D) atoms was used, allowing the pseudo-first-order approximation to be applied. Under these conditions, reagent C(¹D) concentrations varied as a function of reaction time. Typical product H(²S) VUV fluorescence profiles recorded at 296 K are displayed in Figure 1, where the signal intensity is displayed as a function of time, corresponding to the photolysis laser-probe laser delay.

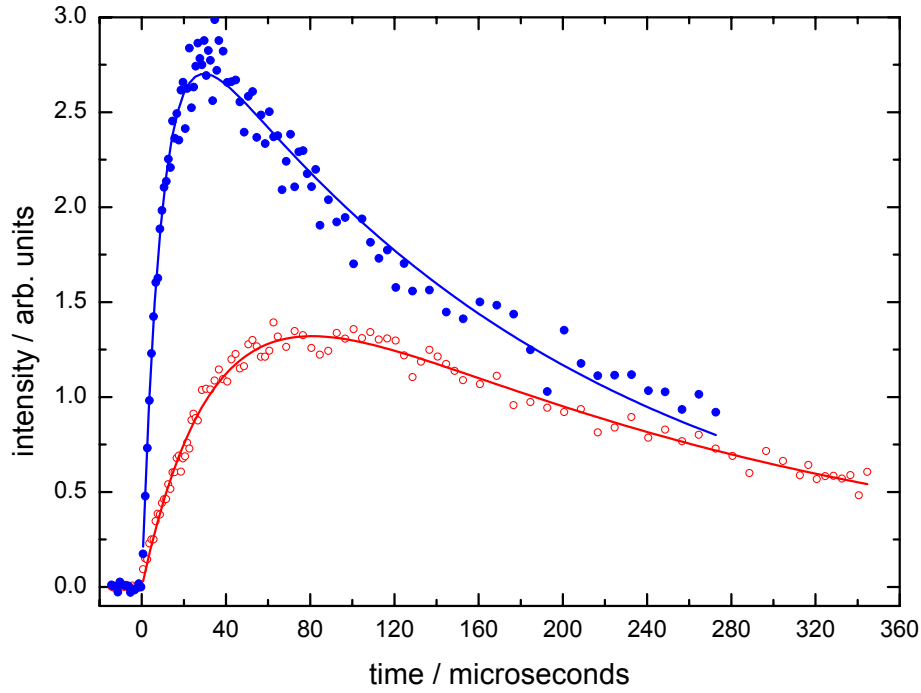


Figure 1 H(²S) atom VUV LIF intensity as a function of time produced by the C(¹D) + H₂O reaction at 296 K. (Blue solid circles) [H₂O] = 2.7 × 10¹⁴ cm⁻³; (red open circles) [H₂O] = 4.3 × 10¹³ cm⁻³. Biexponential fits to the data of the form presented in equation (1) are shown as solid lines.

As the pseudo-first-order approximation was applied, the H-atom fluorescence signal, I_H , was well described by the following expression

$$I_H = A\{exp(-k_{L(H)}t) - exp(-k't)\} \quad (1)$$

where $k' = k[H_2O] + k_{L(C)}$. Here, k is the second-order rate constant for the C(¹D) + H₂O reaction, $k_{L(C)}$ represents other first-order losses for C(¹D) including secondary reactions and diffusion from the probe volume, [H₂O] is the H₂O concentration, t is time and A is the signal amplitude. The first exponential term in expression (1) represents H-atom losses with a first-order rate constant $k_{L(H)}$ and is thought to be mostly due to diffusion from the probe volume.

Decay curves were recorded over a range of $[\text{H}_2\text{O}]$ for any particular temperature, yielding several values of the pseudo-first-order rate constant k' . Plots of k' versus $[\text{H}_2\text{O}]$ were then used to extract the second-order rate constants for a particular temperature. To account for statistical uncertainties on the measured k' values, the second-order rate constants were derived by weighted linear least-squares fits. Here, the individual datapoints were weighted by the reciprocal of the square of the uncertainty value. Figure 2 shows two second-order plots with their associated fits recorded at 75 K and at 296 K.

Figure 2 Pseudo-first order rate constants as a function of $[\text{H}_2\text{O}]$ for the $\text{C}(^1\text{D}) + \text{H}_2\text{O}$ reaction. (red solid circles) data recorded at 296 K; (blue solid triangles) data recorded at 75 K. Error bars represent the statistical uncertainties of the measured k' values derived from biexponential fits. Weighted fits to the datasets (as described in the text) are shown as solid blue and red lines.

As can be seen in Fig 2, the water concentrations used at low temperature are considerably smaller than those used during room temperature experiments. In previous work, H_2O cluster formation (as interpreted by curvature in the second-order plots at high $[\text{H}_2\text{O}]$) provided clear constraints to limit the range of useable water concentrations. The second-order rate constants for the $\text{C}(^1\text{D}) + \text{H}_2\text{O}$ reaction over the 75 K – 296 K range are listed in Table 1, while Figure 3 displays these rate constants as a function of temperature.

Table 1 Measured rate constants for the $\text{C}(^1\text{D}) + \text{H}_2\text{O}$ reaction

T / K	N^b	$[\text{H}_2\text{O}] / 10^{13} \text{ cm}^{-3}$	$k_{\text{C}(^1\text{D})+\text{H}_2\text{O}} / \text{cm}^3 \text{ s}^{-1}$
296	35	4.3 – 27.0	$(3.3 \pm 0.4)^c \times 10^{-10}$
127 ± 2^a	39	3.3 – 18.2	$(3.7 \pm 0.4) \times 10^{-10}$

75 ± 2	30	1.0 – 8.2	$(4.0 \pm 0.4) \times 10^{-10}$
------------	----	-----------	---------------------------------

^aErrors (1σ) on the calculated temperatures are derived from Pitot tube measurements of the impact pressure as a function of distance. ^bNumber of individual measurements. ^cErrors on the rate constants represent both statistical and systematic errors as explained in the text.

To place realistic error bars on the measured second-order rate constants, the statistical uncertainties derived from fits similar to those shown in Figure 2 were combined with an estimated systematic error, fixed to 10 % of the value of the nominal rate constant. These systematic errors could have arisen from equipment calibration errors (mass-flow controllers, pressure gauges, etc) as well as potential errors in the calculated supersonic flow properties (density and velocity).

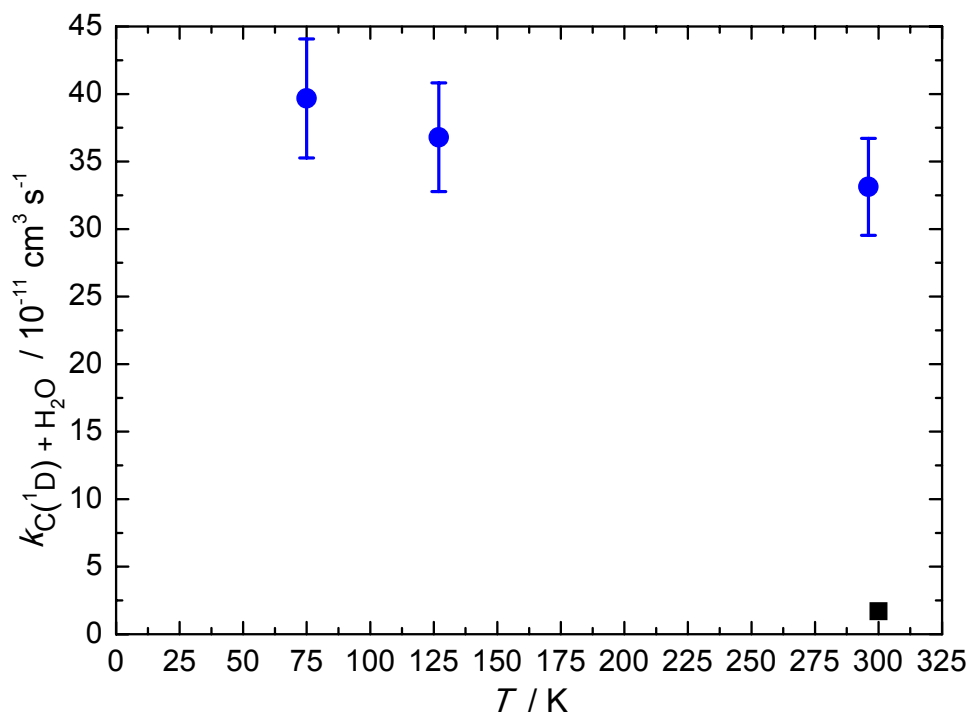


Figure 3 Rate constants for the $C(^1D) + H_2O$ reaction as a function of temperature. (dark blue circles) this work; (solid black square) Husain & Kirsch³³. Error bars represent the combined statistical and systematic errors (see text for details).

Husain and Kirsch³³ obtained a rate constant of $1.7 \times 10^{-11} \text{ cm}^3 \text{ s}^{-1}$ at 300 K in their earlier investigation of the $C(^1D) + H_2O$ reaction; a value that is almost twenty times smaller than the one derived in the present investigation at room temperature. These authors, who employed the flash photolysis of carbon suboxide C_3O_2 at wavelengths greater than 105 nm as the source of $C(^1D)$ atoms in their experiments, suggest that this particular result could be of limited accuracy due to the extent of water photolysis that occurred simultaneously in their apparatus.

When similar experiments to those described above were performed at 50 K, H-atom fluorescence profiles such as those shown in Fig. 4A were recorded instead. Although decays similar to those shown in Fig. 1 are obtained when low $[H_2O]$ is used ($2.6 \times 10^{13} \text{ cm}^{-3}$ in Fig 4A), when higher $[H_2O]$ values were employed ($8.8 \times 10^{13} \text{ cm}^{-3}$ in Fig 4A), the long-time part of the H-atom fluorescence curve was seen to increase rather than decaying slowly back to zero, yielding a non-physical negative value for the H-atom loss term in equation (1). This observation can be interpreted as being due to the production of H-atoms over a longer timescale by the reaction of ground state $C(^3P)$ atoms with H_2O , arising from the presence of significant quantities of $C(^3P)$ atoms in the supersonic flow. In earlier work, Hickson et al.⁴ showed that the rate constant for the $C(^3P) + H_2O \rightarrow H + HCO$ reaction increases markedly below 100 K as a result of quantum tunneling, reaching a value of $3.6 \times 10^{-11} \text{ cm}^3 \text{ s}^{-1}$ at 50 K. Consequently, it was impossible to use the recorded H-atom formation curves at 50 K to extract rate information. Given the potential for significant interference with the kinetic measurements of the $C(^1D) + H_2O$ reaction at other temperatures, it was also necessary to examine the kinetic

data recorded at 75 K and 127 K to quantify the extent of H-atom production by the ground state carbon atom reaction in these cases. Figs. 4B and 4C show kinetic data recorded at 75 K and 127 K respectively, in the presence of both high and low $[\text{H}_2\text{O}]$. The curves displayed here represent the lowest and highest $[\text{H}_2\text{O}]$ used at these temperatures, allowing us to compare the long-time behavior of the H-atom fluorescence signal (which should be most affected in the event of H-atom production by the $\text{C}(^3\text{P}) + \text{H}_2\text{O}$ reaction). At 127 K (panel C), the long-time part of the H-atom profiles are essentially the same for both $[\text{H}_2\text{O}]$ (as confirmed by the similar $k_{L(H)}$ values yielded by biexponential fits), indicating the negligible contribution of secondary H-atom production at this temperature. This finding is in good agreement with the earlier results of Hickson et al. who derived a rate constant for the $\text{C}(^3\text{P}) + \text{H}_2\text{O}$ reaction at 106 K of $4.9 \times 10^{-12} \text{ cm}^3 \text{ s}^{-1}$.⁴ At 75 K, it can be seen that the long-time part of the H-atom profiles are somewhat different at high and low $[\text{H}_2\text{O}]$, with slightly smaller $k_{L(H)}$ values when $[\text{H}_2\text{O}]$ is large. As the rate constant for the $\text{C}(^3\text{P}) + \text{H}_2\text{O}$ reaction is considerably larger at this temperature ($\sim 1.2 \times 10^{-11} \text{ cm}^3 \text{ s}^{-1}$)⁴ there might be a small secondary contribution to H-atom production.

In order to quantify the possible effects of the $\text{C}(^3\text{P}) + \text{H}_2\text{O}$ reaction on the target reaction kinetics, numerical simulations of the reactive system were performed at 75 K and 127 K, following H-atom production using the differential integrator FACSIMILE. Here, the $\text{C}(^1\text{D})/(\text{C}(^3\text{P})+\text{C}(^1\text{D}))$ branching fraction for CBr_4 photolysis was considered to be equal to 0.1 and the rate constants for the $\text{C}(^3\text{P}) + \text{H}_2\text{O}$ reaction were set to the values measured by Hickson et al.⁴ (the value recorded at 106 K was used to represent the rate constant at 127 K although this is likely to be an overestimate of the real rate constant). Temporal profiles such as those displayed in Fig 3 were simulated for the same range of $[\text{H}_2\text{O}]$ used in the experiments. Biexponential fits to these profiles allowed us to extract the pseudo-first-order rate constants which were plotted against the corresponding $[\text{H}_2\text{O}]$ to yield the simulated second-order rate constant. Finally, these output values were compared with the simulation input values to see if

significant deviations in the $C(^1D) + H_2O$ rate constant occurred. At both 75 K and 127 K, the simulated second-order rate constants for the $C(^1D) + H_2O$ reaction are approximately 25 % smaller than the input values, with curvature appearing in the second-order plots at high $[H_2O]$. As no curvature was ever observed in any of the experimental second-order plots (see Fig. 2), it is possible that these initial simulations overestimate secondary H-atom production from the $C(^3P) + H_2O$ reaction and/or underestimate H-atom production from the $C(^1D) + H_2O$ reaction. Indeed, if a $C(^1D)/(C(^3P)+C(^1D))$ ratio of 0.2 is used instead (the measured value was 0.1-0.15),⁷ the discrepancy decreases to 10 % in both cases. Moreover, if the $C(^3P) + H_2O$ rate constant is also reduced by 50% (to take into account the fact that a significant fraction of the total rate constant involves complex stabilization rather than reaction, as previously observed at 50 K⁴), the derived $C(^1D) + H_2O$ values are now only 5% smaller than the input values. As secondary H-atom formation at these temperatures is relatively weak (as shown by linear second-order plots at all temperatures above 50 K) it is expected that the differences between the real rate constants and the ones derived here should be small.

Assuming that the measured low temperature rate constants accurately reflect the real ones, it can be seen that the reaction rate increases as the temperature falls, displaying a slightly negative dependence on temperature to reach a value of $(4.0 \pm 0.4) \times 10^{-10} \text{ cm}^3 \text{ s}^{-1}$ at 75 K. Such large values of the rate constant are a clear indication that reaction occurs for essentially every collision between reagents.

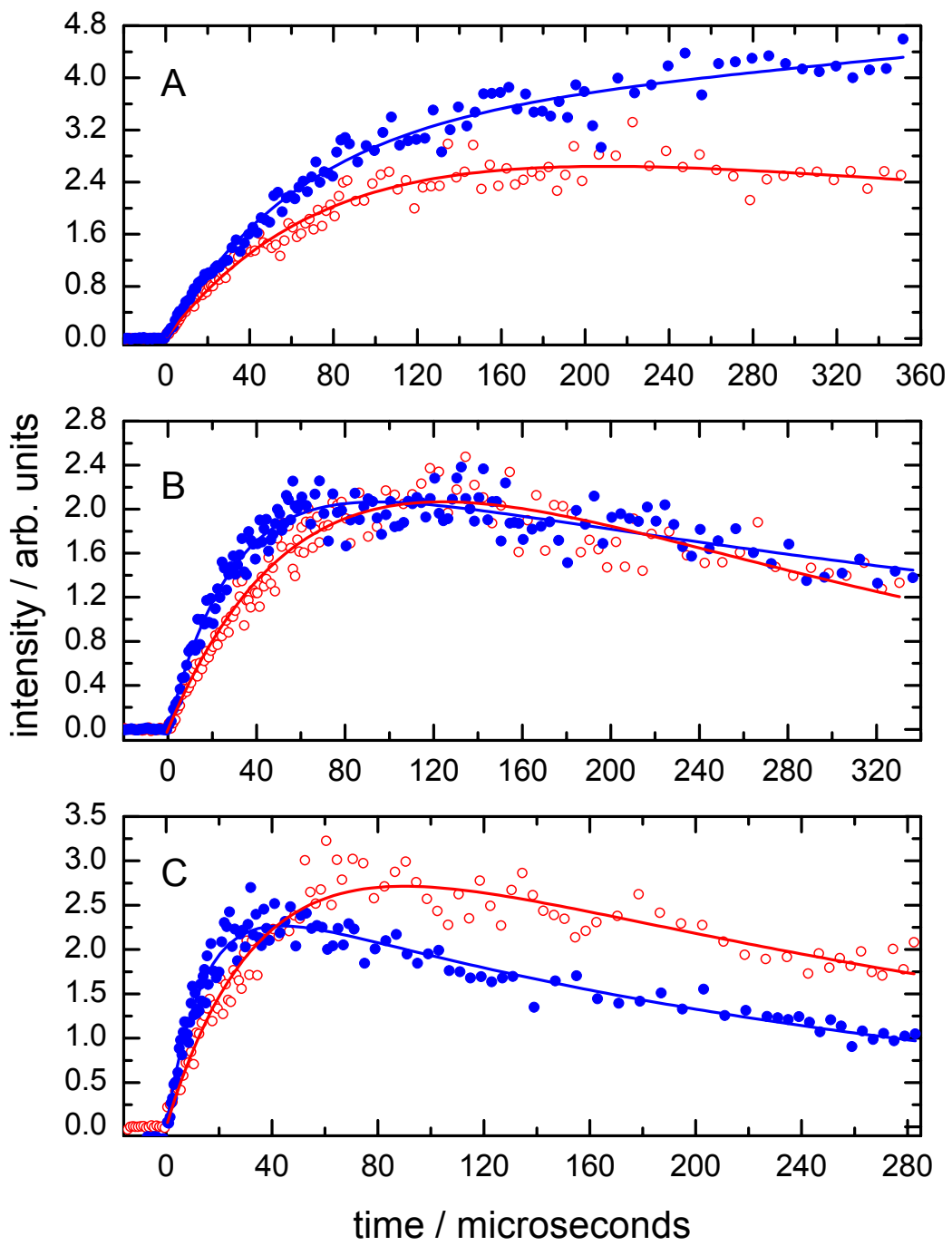


Figure 4 H-atom VUV LIF intensity as a function of time recorded at 3 different temperatures. **A** 50 K data: (Blue solid circles) $[\text{H}_2\text{O}] = 8.8 \times 10^{13} \text{ cm}^{-3}$; (red open circles) $[\text{H}_2\text{O}] = 2.6 \times 10^{13} \text{ cm}^{-3}$; **B** 75 K data: (Blue solid circles) $[\text{H}_2\text{O}] = 8.2 \times 10^{13} \text{ cm}^{-3}$; (red open circles) $[\text{H}_2\text{O}] = 2.4 \times 10^{13} \text{ cm}^{-3}$; **C** 127 K data: (Blue solid circles) $[\text{H}_2\text{O}] = 1.7 \times 10^{14} \text{ cm}^{-3}$; (red open circles) $[\text{H}_2\text{O}] = 3.3 \times 10^{13} \text{ cm}^{-3}$. Solid blue and red lines represent biexponential fits to the individual temporal profiles.

Temperature dependent H-atom yields

To determine absolute H-atom yields over the 50-296 K temperature range, the H-atom VUV LIF signal from the target $\text{C}(^1\text{D}) + \text{H}_2\text{O}$ reaction was calibrated using the $\text{C}(^1\text{D}) + \text{H}_2$ reference reaction; a process which is assumed to produce atomic hydrogen with a 100 % yield over the entire temperature range. During these experiments, VUV LIF signals were recorded as a function of delay time between the photolysis laser and the probe laser in an identical manner to the experiments performed to obtain temperature dependent rate constants. To ensure that $\text{C}(^1\text{D})$ losses did not lead to large errors in the estimation of the H-atom yields, only profiles with similar time constants were used to extract relative intensities. In this case, as $k_{\text{L}(\text{C})}$ is the same for the target and reference reactions, relative H-atom intensities can be compared directly. As a result, excess reagent concentrations (H_2 or H_2O) were carefully chosen to obtain comparable first-order-production rates for both reactions. To lower the measurement uncertainty, at least eight pairs of curves were recorded sequentially at each temperature. Additionally, the order in which the profiles were acquired was varied to limit potential errors arising from signal drift as a function of experiment time. 30 datapoints were recorded at each time point, with each formation curve comprising more than 50 time intervals. The baseline level was set by recording several datapoints with the probe laser firing before the photolysis laser. Biexponential fits of the form given by equation (1) were used to extract values for the

signal amplitude A for both the target and reference reactions. Typical examples of the H-atom VUV LIF profiles recorded sequentially are shown in Fig 5.

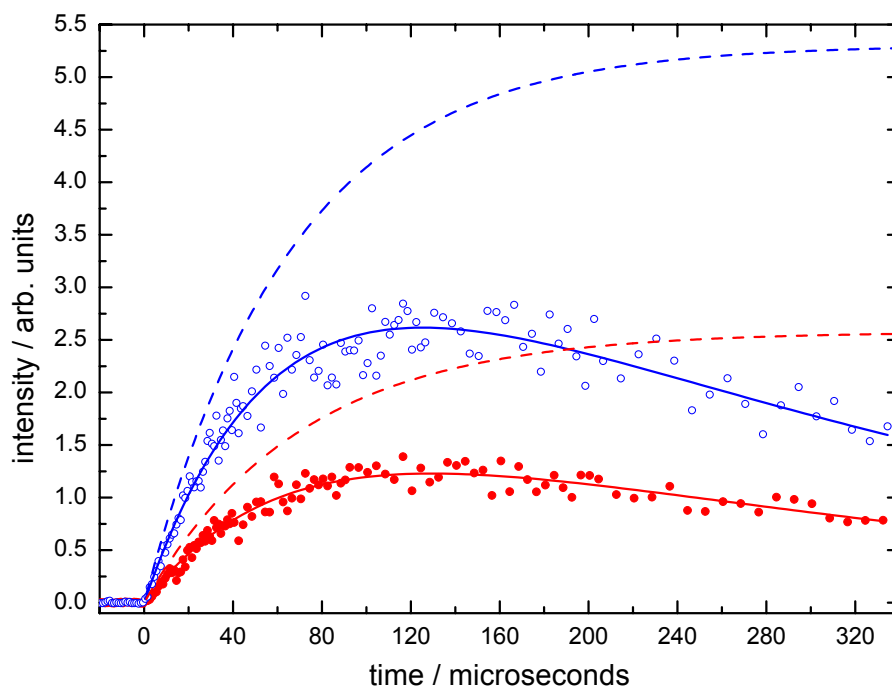


Figure 5. H(²S) VUV LIF emission profiles at 75 K. (Blue open circles) H-atom signal from the C(¹D) + H₂O reaction with [H₂O] = 3.3 × 10¹³ cm⁻³; (blue solid line) biexponential fit to the C(¹D) + H₂O reaction H-atom data; (blue dashed line) theoretical H-atom yield from the C(¹D) + H₂O reaction without H-atom losses. (Red solid circles) H-atom signal from the C(¹D) + H₂ reaction with [H₂] = 4.7 × 10¹³ cm⁻³; (red solid line) biexponential fit to the C(¹D) + H₂ reaction H-atom data; (red dashed line) theoretical H-atom yield from the C(¹D) + H₂ reaction without H-atom losses.

The expected intensities in the absence of H-atom losses (as obtained by setting the $k_{L(H)}$ parameter equal to zero in equation (1)) are also plotted in Fig. 5. The derived A values were corrected for secondary absorption of the VUV source and signal intensities by residual H₂O

and H₂ within the reactor. Secondary absorption by H₂ was negligible for all experiments, whereas the correction for experiments employing H₂O was greatest at room temperature with a value of less than 3 %. Below room temperature, the H₂O correction was at most 1 %. The derived H-atom yields are listed in Table 2 and are presented as a function of temperature in Fig. 6.

Table 2 H-atom yields for the C(¹D) + H₂O reaction as a function of temperature

T / K	Number of experiments	$k_{L(C)} / s^{-1}$	H-atom yield
296	16	14700 ± 1500^a	1.82 ± 0.08^B
127	9	12200 ± 1400	1.93 ± 0.11
75	8	4400 ± 700	2.04 ± 0.14
50	8		3.17 ± 0.11

^aValues derived from the y-axis intercept of second-order plots such as those shown in Fig. 2.

^bErrors are cited at the 95 % confidence level.

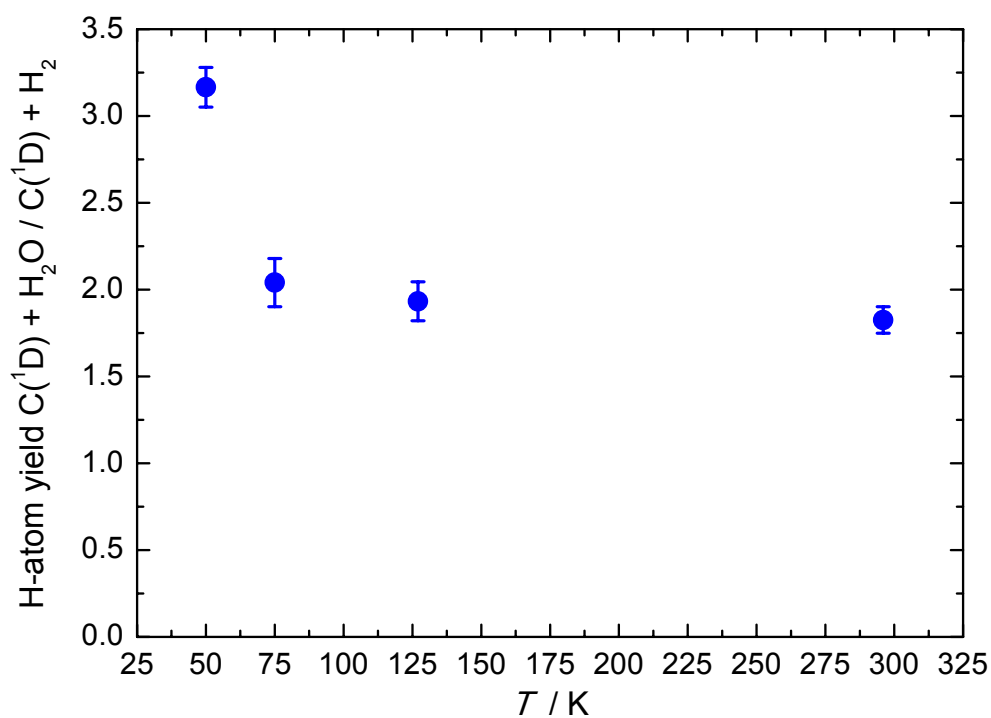


Figure 6 Absolute H-atom yields of the $C(^1D) + H_2O$ reaction as a function of temperature. The large value derived at 50 K is probably due to supplementary H-atom formation from the $C(^3P) + H_2O$ reaction.

In the absence of secondary chemistry, the maximum absolute H-atom yield from the $C(^1D) + H_2O$ reaction is limited to 2, given the possibility to liberate the two H-atoms of the water molecule. A significant fraction of the available excess energy (due to the large exothermicity of the excited state atom reaction) is expected to be carried away as internal excitation of the molecular formyl (HCO) and/or isoformyl (COH) coproducts, which clearly dissociate with a high probability to yield a second H-atom. Indeed, at room temperature, the derived H-atom yield of 1.82 ± 0.08 is already close to the theoretical maximum. According to the calculations of Ozkan and Dede,⁴⁴ reaction could occur through several direct pathways (with the formation of ground S_0 and excited singlet S_1 hydroxymethylene species as intermediates) as well as possible indirect ones (via intersystem crossing to the triplet T_1 hydroxymethylene surface). These authors state that given the large excess of available energy, the expected major gas-phase products should be $CO + H + H$ with only a small contribution from $H_2 + CO$ via cis-hydroxymethylene and formaldehyde intermediates; a hypothesis that is confirmed by the present room temperature results. In common with other strongly exothermic reactions,^{7, 8} it is not expected that the product yields vary significantly as a function of temperature, at least over the range investigated during these experiments. Nevertheless, it can be seen from both Table 2 and Fig. 6 that the low temperature H-atom yields are greater than both the room temperature value and the theoretical maximum value below 100 K. At 50 K, the much larger H-atom yield of 3.17 ± 0.11 can be attributed to supplementary atomic hydrogen production by the $C(^3P) + H_2O \rightarrow H + HCO$ reaction, due to the presence of substantial quantities of ground state atomic carbon in the supersonic flow and this result provides clear supplementary evidence for the role

of quantum tunneling in this activated reaction. Moreover, as the H-atom yields obtained at both 75 K and 127 K are also slightly greater than those obtained at 296 K (for which little or no tunneling is expected in the reaction of ground state carbon atoms with water), it is possible that some quantum tunneling could also be occurring at these intermediate temperatures. Although Hickson et al.⁴ derived quantitative H-atom yields from the $C(^3P) + H_2O$ reaction at 50 K, these authors were unable to quantify the extent of tunneling at higher temperatures. In contrast, the present work provides possible qualitative evidence for tunneling at 75 K (the measured H-atom yield of 2.04 ± 0.14 is at the limit of the combined error bars considering the room temperature value), while the measured H-atom yield at 127 K might even be indicative of a small tunneling contribution at this temperature.

4 Conclusions

Here the results of a low temperature study of the kinetics of the barrierless $C(^1D) + H_2O$ reaction are presented, based on the use of a Laval nozzle reactor. Excited state $C(^1D)$ atoms were created by the pulsed laser photolysis of CBr_4 ; a process which simultaneously generates ground state $C(^3P)$ atoms. As $C(^1D)$ could not be detected directly, atomic hydrogen product formation was followed instead by vacuum ultraviolet laser induced fluorescence allowing second-order rate constants and absolute H-atom yields to be determined. The measured rate constants are large and display a slight negative temperature dependence down to 75 K, while the measured H-atom yields are close to the theoretical maximum value of two above 100 K. At 50 K, kinetic measurements could not be exploited, while the derived H-atom yields at this temperature significantly exceeded the theoretical maximum value. These results are consistent with an additional source of atomic hydrogen at low temperature, namely the activated $C(^3P) + H_2O$ reaction that has already been shown to proceed by quantum tunneling in earlier work. The derived H-atom yields at 75 K (and to a lesser extent those recorded at 127 K) indicate that quantum tunneling might also play a role at these intermediate temperatures.

AUTHOR INFORMATION

Corresponding Author

* Correspondence to: kevin.hickson@u-bordeaux.fr. Tel: +33 (0)5 40 00 63 42

Acknowledgements

K.M.H. acknowledges support from the French program “Physique et Chimie du Milieu Interstellaire” (PCMI) of the CNRS/INSU with the INC/INP co-funded by the CEA and CNES as well as funding from the "Program National de Planétologie" (PNP) of the CNRS/INSU.

References

1. Clary, D. C.; Haider, N.; Husain, D.; Kabir, M. Interstellar Carbon Chemistry: Reaction Rates of Neutral Atomic Carbon with Organic Molecules. *Astrophys. J.* **1994**, *422*, 416-422.
2. Chastaing, D.; James, P. L.; Sims, I. R.; Smith, I. W. M. Neutral-Neutral Reactions at the Temperatures of Interstellar Clouds: Rate Coefficients for Reactions of Atomic Carbon, C(³P), with O₂, C₂H₂, C₂H₄ and C₃H₆ Down to 15 K. *Phys. Chem. Chem. Phys.* **1999**, *1*, 2247-2256.
3. Chastaing, D.; Le Picard, S. D.; Sims, I. R. Direct Kinetic Measurements on Reactions of Atomic Carbon, C(³P), with O₂ and NO at Temperatures Down to 15 K. *J. Chem. Phys.* **2000**, *112*, 8466-8469.
4. Hickson, K. M.; Loison, J.-C.; Nuñez-Reyes, D.; Méreau, R. Quantum Tunneling Enhancement of the C + H₂O and C + D₂O Reactions at Low Temperature. *J. Phys. Chem. Lett.* **2016**, *7*, 3641-3646.
5. Hickson, K. M.; Loison, J.-C.; Wakelam, V. Temperature Dependent Product Yields for the Spin Forbidden Singlet Channel of the C(³P) + C₂H₂ Reaction. *Chem. Phys. Lett.* **2016**, *659*, 70-75.

6. Hickson, K. M.; Loison, J.-C.; Bourgalais, J.; Capron, M.; Picard, S. D.; Goulay, F.; Wakelam, V. The C(³P) + NH₃ reaction in Interstellar Chemistry. II. Low Temperature Rate Constants and Modeling of NH, NH₂, and NH₃ Abundances in Dense Interstellar Clouds. *Astrophys. J.* **2015**, *812*, 107.
7. Shannon, R. J.; Cossou, C.; Loison, J.-C.; Caubet, P.; Balucani, N.; Seakins, P. W.; Wakelam, V.; Hickson, K. M. The Fast C(³P) + CH₃OH Reaction as an Efficient Loss Process for Gas-Phase Interstellar Methanol. *RSC Adv.* **2014**, *4*, 26342-26353.
8. Bourgalais, J.; Capron, M.; Kailasanathan, R. K. A.; Osborn, D. L.; Hickson, K. M.; Loison, J.-C.; Wakelam, V.; Goulay, F.; Le Picard, S. D. The C(³P) + NH₃ Reaction in Interstellar Chemistry. I. Investigation of the Product Formation Channels. *Astrophys. J.* **2015**, *812*, 106.
9. Clary, D. C.; Buonomo, E.; Sims, I. R.; Smith, I. W. M.; Geppert, W. D.; Naulin, C.; Costes, M.; Cartechini, L.; Casavecchia, P. C + C₂H₂: A Key Reaction in Interstellar Chemistry. *J. Phys. Chem. A* **2002**, *106*, 5541-5552.
10. Kaiser, R. I.; Ochsenfeld, C.; Head-Gordon, M.; Lee, Y. T.; Suits, A. G. Crossed-Beam Reaction of Carbon Atoms with Hydrocarbon Molecules. III: Chemical Dynamics of Propynylidyne (l-C₃H; X²Π_j) and Cyclopropynylidyne (c-C₃H; X²B₂) Formation from Reaction of C(³P_j) with Acetylene, C₂H₂(X 1Σ_g⁺). *J. Chem. Phys.* **1997**, *106*, 1729-1741.
11. Costes, M.; Halvick, P.; Hickson, K. M.; Daugey, N.; Naulin, C. Non-Threshold, Threshold, and Nonadiabatic Behavior of the Key Interstellar C + C₂H₂ Reaction. *Astrophys. J.* **2009**, *703*, 1179-1187.
12. Naulin, C.; Daugey, N.; Hickson, K. M.; Costes, M. Dynamics of the Reactions of C(³P_j) Atoms with Ethylene, Allene, and Methylacetylene at Low Energy Revealed by Doppler–Fizeau Spectroscopy. *J. Phys. Chem. A* **2009**, *113*, 14447-14457.

13. Leonori, F.; Petrucci, R.; Segoloni, E.; Bergeat, A.; Hickson, K. M.; Balucani, N.; Casavecchia, P. Unraveling the Dynamics of the $C(^3P,^1D) + C_2H_2$ Reactions by the Crossed Molecular Beam Scattering Technique. *J. Phys. Chem. A* **2008**, *112*, 1363-1379.
14. Balucani, N.; Capozza, G.; Cartechini, L.; Bergeat, A.; Bobbenkamp, R.; Casavecchia, P.; Javier Aoiz, F.; Bañares, L.; Honvault, P.; Bussery-Honvault, B., et al. Dynamics of the Insertion Reaction $C(^1D) + H_2$: A Comparison of Crossed Molecular Beam Experiments with Quasiclassical Trajectory and Quantum Mechanical Scattering Calculations. *Phys. Chem. Chem. Phys.* **2004**, *6*, 4957-4967.
15. Balucani, N.; Casavecchia, P.; Aoiz, F. J.; Bañares, L.; Launay, J.-M.; Bussery-Honvault, B.; Honvault, P. Dynamics of the $C(^1D) + H_2$ reaction: A Comparison of Crossed Molecular Beam Experiments with Quantum Mechanical and Quasiclassical Trajectory Calculations on the First Two Singlet ($1^1A'$ and $1^1A''$) Potential Energy Surfaces. *Mol. Phys.* **2010**, *108*, 373-380.
16. Bergeat, A.; Cartechini, L.; Balucani, N.; Capozza, G.; Phillips, L. F.; Casavecchia, P.; Volpi, G. G.; Bonnet, L.; Rayez, J. C. A Crossed-Beam Study of the Reaction $C(^1D) + H_2(X^1\Sigma^+, v = 0) \rightarrow CH(X^2\Pi, v') + H(^2S)$. *Chem. Phys. Lett.* **2000**, *327*, 197-202.
17. Bussery-Honvault, B.; Honvault, P.; Launay, J. M. A Study of the $C(^1D) + H_2 \rightarrow CH + H$ Reaction: Global Potential Energy Surface and Quantum Dynamics. *J. Chem. Phys.* **2001**, *115*, 10701-10708.
18. Bussery-Honvault, B.; Julien, J.; Honvault, P.; Launay, J.-M. Global $1^1A''$ Potential Energy Surface of CH_2 and Quantum Dynamics of a Sideways Insertion Mechanism for the $C(^1D) + H_2 \rightarrow CH(^2\Pi) + H$ Reaction. *Phys. Chem. Chem. Phys.* **2005**, *7*, 1476-1481.
19. Defazio, P.; Petrongolo, C.; Bussery-Honvault, B.; Honvault, P. Born-Oppenheimer Quantum Dynamics of the $C(^1D) + H_2$ Reaction on the $CH_2 \tilde{a}^1A_1$ and \tilde{b}^1B_1 Surfaces. *J. Chem. Phys.* **2009**, *131*, 114303.

20. Defazio, P.; Bussery-Honvault, B.; Honvault, P.; Petrongolo, C. Nonadiabatic Quantum Dynamics of $C(^1D) + H_2 \rightarrow CH + H$: Coupled-Channel Calculations Including Renner-Teller and Coriolis Terms. *J. Chem. Phys.* **2011**, *135*, 114308.
21. Lin, S. Y.; Guo, H. Reactions of $C(^1D)$ with H_2 and its Deuterated Isotopomers, a Wave Packet Study. *J. Chem. Phys.* **2004**, *121*, 1285-1292.
22. Lin, S. Y.; Guo, H. Quantum Wave Packet Study of Reactive and Inelastic Scattering between $C(^1D)$ and H_2 . *J. Chem. Phys.* **2003**, *119*, 11602-11608.
23. Lin, S. Y.; Guo, H. Quantum Wave Packet Studies of the $C(^1D) + H_2 \rightarrow CH + H$ Reaction: Integral Cross Section and Rate Constant. *J. Phys. Chem. A* **2004**, *108*, 2141-2148.
24. Liu, J.; Fu, B.; Zhang, D. Quantum Wave Packet Study of the $C(^1D) + H_2$ Reaction. *Chem. Phys. Lett.* **2009**, *480*, 46-48.
25. Shen, Z.; Cao, J.; Bian, W. Quantum Mechanical Differential and Integral Cross Sections for the $C(^1D) + H_2 (v = 0, j = 0) \rightarrow CH(v', j') + H$ Reaction. *J. Chem. Phys.* **2015**, *142*, 164309.
26. Sun, Z.; Zhang, C.; Lin, S.; Zheng, Y.; Meng, Q.; Bian, W. Quantum Reaction Dynamics of the $C(^1D) + H_2(D_2) \rightarrow CH(D) + H(D)$ on a New Potential Energy Surface. *J. Chem. Phys.* **2013**, *139*, 014306.
27. Leonori, F.; Skouteris, D.; Petrucci, R.; Casavecchia, P.; Rosi, M.; Balucani, N. Combined Crossed Beam and Theoretical Studies of the $C(^1D) + CH_4$ Reaction. *J. Chem. Phys.* **2013**, *138*, 024311.
28. Scott, D. C.; De Juan, J.; Robie, D. C.; Schwartz-Lavi, D.; Reisler, H. Reactions of $C(^1D)$ with H_2 and HCl : Product State Excitations, Λ -Doublet Propensities, and Branching Ratios. *J. Phys. Chem.* **1992**, *96*, 2509-2518.
29. Jursich, G. M.; Wiesenfeld, J. R. Product Energetics of the Reaction $C(^1D) + H_2 \rightarrow CH + H$. *Chem. Phys. Lett.* **1984**, *110*, 14-19.

30. Cartechini, L.; Bergeat, A.; Capozza, G.; Casavecchia, P.; Volpi, G. G.; Geppert, W. D.; Naulin, C.; Costes, M. Dynamics of the C + C₂H₂ Reaction from Differential and Integral Cross-Section Measurements in Crossed-Beam Experiments. *J. Chem. Phys.* **2002**, *116*, 5603-5611.
31. Donovan, R. J.; Husain, D. Recent Advances in the Chemistry of Electronically Excited Atoms. *Chem. Rev.* **1970**, *70*, 489-516.
32. Husain, D.; Kirsch, L. J. Study of Electronically Excited Carbon Atoms, C(2¹D₂), by the Attenuation of Atomic Emission, (3¹P₁^o → 2¹D₂). Part 1.-Collisional Deactivation of C(2¹D₂) by the Noble Gases. *Trans. Faraday Soc.* **1971**, *67*, 2886-2895.
33. Husain, D.; Kirsch, L. J. Study of Electronically Excited Carbon Atoms, C(2¹D₂), by Time-Resolved Atomic Absorption at 193.1 nm, (3¹P₁^o → 2¹D₂) .2. Reactions of C(2¹D₂) with Molecules. *Trans. Faraday Soc.* **1971**, *67*, 3166-3175.
34. Fisher, W. H.; Carrington, T.; Sadowski, C. M.; Dugan, C. H. The Reactions of C(2¹D₂) with H₂, D₂ and HD: Product Rotational Energies, Isotope Effects and the CD/CH Branching Ratio. *Chem. Phys.* **1985**, *97*, 433-448.
35. Husain, D.; Kirsch, L. J. The Study of Electronically Excited Carbon Atoms, C(2¹D₂), by Photoelectric Measurement of Time-Resolved Atomic Absorption. *Chem. Phys. Lett.* **1971**, *9*, 412-415.
36. Sato, K.; Ishida, N.; Kurakata, T.; Iwasaki, A.; Tsnuashima, S. Reactions of C(¹D) with H₂, HD and D₂ : Kinetic Isotope Effect and the CD/CH Branching Ratio. *Chem. Phys.* **1998**, *237*, 195-204.
37. Hickson, K. M.; Loison, J. C.; Guo, H.; Suleimanov, Y. V. Ring-Polymer Molecular Dynamics for the Prediction of Low-Temperature Rates: An Investigation of the C(¹D) + H₂ Reaction. *J. Phys. Chem. Lett.* **2015**, *6*, 4194-4199.

38. Hickson, K. M.; Suleimanov, Y. V. An Experimental and Theoretical Investigation of the C(¹D) + D₂ Reaction. *Phys. Chem. Chem. Phys.* **2017**, *19*, 480-486.
39. Wu, Y.; Cao, J.; Ma, H.; Zhang, C.; Bian, W.; Nuñez-Reyes, D.; Hickson, K. M. Conical Intersection-Regulated Intermediates in Bimolecular Reactions: Insights from C(¹D) + HD Dynamics. *Sci. Adv.* **2019**, *5*, EAAW0446.
40. Nuñez-Reyes, D.; Hickson, K. M. Kinetic and Product Study of the Reactions of C(¹D) with CH₄ and C₂H₆ at Low Temperature. *J. Phys. Chem. A* **2017**, *121*, 3851-3857.
41. Nuñez-Reyes, D.; Hickson, K. M. The Reactivity of C(¹D) with Oxygen Bearing Molecules NO and O₂ at Low Temperature. *Chem. Phys. Lett.* **2017**, *687*, 330-335.
42. Nuñez-Reyes, D.; Hickson, K. M. Kinetics of the Gas-Phase O(¹D) + CO₂ and C(¹D) + CO₂ Reactions over the 50–296 K Range. *J. Phys. Chem. A* **2018**, *122*, 4002-4008.
43. Hickson, K. M.; Loison, J.-C.; Lique, F.; Klos, J. An Experimental and Theoretical Investigation of the C(¹D) + N₂ → C(³P) + N₂ Quenching Reaction at Low Temperature. *J. Phys. Chem. A* **2016**, *120*, 2504-2513.
44. Ozkan, I.; Dede, Y. Reactions of ¹S, ¹D, and ³P Carbon Atoms with Water. Oxygen Abstraction and Intermolecular Formaldehyde Generation Mechanisms; an MCSCF Study. *Int. J. Quantum. Chem.* **2012**, *112*, 1165-1184.
45. Dobrijevic, M.; Hébrard, E.; Loison, J. C.; Hickson, K. M. Coupling of Oxygen, Nitrogen, and Hydrocarbon Species in the Photochemistry of Titan's Atmosphere. *Icarus* **2014**, *228*, 324-346.
46. Hébrard, E.; Dobrijevic, M.; Loison, J. C.; Bergeat, A.; Hickson, K. M.; Caralp, F. Photochemistry of C₃H_p hydrocarbons in Titan's Stratosphere Revisited. *Astron. Astrophys.* **2013**, *552*, A132.
47. Hwang, D. Y.; Mebel, A. M.; Wang, B. C. Ab Initio Study of the Addition of Atomic Carbon with Water. *Chem. Phys.* **1999**, *244*, 143-149.

48. Schreiner, P. R.; Reisenauer, H. P. The "Non-Reaction" of Ground-State Triplet Carbon Atoms with Water Revisited. *ChemPhysChem* **2006**, *7*, 880-885.
49. Ahmed, S. N.; McKee, M. L.; Shevlin, P. B. An Experimental and Ab Initio Study of the Addition of Atomic Carbon to Water. *J. Am. Chem. Soc.* **1983**, *105*, 3942-3947.
50. Husain, D.; Kirsch, L. J. Reactions of Atomic Carbon C(2^3P_j) by Kinetic Absorption Spectroscopy in the Vacuum Ultra-Violet. *J. Chem. Soc. Faraday Trans.* **1971**, *67*, 2025-2035.
51. Husain, D.; Young, A. N. Kinetic Investigation of Ground State Carbon Atoms, C($3P$). *J. Chem. Soc. Faraday Trans. 2* **1975**, *71*, 525-531.
52. Daugey, N.; Caubet, P.; Retail, B.; Costes, M.; Bergeat, A.; Dorthe, G. Kinetic Measurements on Methylidyne Radical Reactions with Several Hydrocarbons at Low Temperatures. *Phys. Chem. Chem. Phys.* **2005**, *7*, 2921-2927.
53. Daugey, N.; Caubet, P.; Bergeat, A.; Costes, M.; Hickson, K. M. Reaction Kinetics to Low Temperatures. Dicarbon + Acetylene, Methylacetylene, Allene and Propene from $77 \leq T \leq 296$ K. *Phys. Chem. Chem. Phys.* **2008**, *10*, 729-737.
54. Grondin, R.; Loison, J.-C.; Hickson, K. M. Low Temperature Rate Constants for the Reactions of O($1D$) with N₂, O₂ and Ar. *J. Phys. Chem. A* **2016**, *120*, 4838-4844.
55. Sander, S. P.; Abbatt, J.; Barker, J. R.; Burkholder, J. B.; Friedl, R. R.; Golden, D. M.; Huie, R. E.; Kolb, C. E.; Kurylo, M. J.; Moortgat, G. K., et al. Chemical Kinetics and Photochemical Data for Use in Atmospheric Studies, Evaluation No. 17. *JPL Publication 10-6, Jet Propulsion Laboratory, Pasadena, 2011* <http://jpldataeval.jpl.nasa.gov/>. **2011**.
56. Nuñez-Reyes, D.; Hickson, K. M. Rate Constants and H-Atom Product Yields for the Reactions of O($1D$) Atoms with Ethane and Acetylene from 50 to 296 K. *J. Phys. Chem. A* **2018**, *122*, 4696-4703.

TOC Graphic

